Atmos. Chem. Phys. Discuss., https://doi.org/10.5194/acp-2017-668
Manuscript under review for journal Atmos. Chem. Phys.
Discussion started: 1 August 2017

Atmospheric Chemistry and Physics Discussions

High-time resolved radon-progeny measurements in the Arctic region (Svalbard Islands, Norway): results and potentialities

Roberto Salzano[1], Antonello Pasini[2], Antonietta Ianniello[2], Mauro Mazzola[3], Rita Traversi[4], Roberto Udisti[4]

[1]Institute for Atmospheric Pollution Research, National Research Council of Italy, Sesto Fiorentino (FI), Italy
[2]Institute for Atmospheric Pollution Research, National Research Council of Italy, Monterotondo (RM), Italy
[3]Institute of Atmospheric Sciences and Climate, National Research Council of Italy, Bologna (BO), Italy
[4]Department of Chemistry "Ugo Schiff", University of Florence, Sesto Fiorentino (FI), Italy

Correspondence to: Roberto Salzano (roberto.salzano@cnr.it)

Abstract. The estimation of radon progeny in the Arctic region represents a scientific challenge due to the required low limit of detection in consideration of the limited radon emanation associated with permafrost dynamics. This preliminary study highlighted, for the first time, the possibility to monitor radon progeny in the Arctic region with a higher time resolution. The composition of the radon progeny offered the opportunity to identify air masses dominated by long-range transport, in presence or not of near-constant radon progeny instead of long and short lived progenies. Furthermore, the different ratio between radon and thoron progenies evidenced the contributions of local emissions and atmospheric stability. Two different emanation periods were defined in accordance to the permafrost dynamics at the ground and several accumulation windows were recognized coherently to the meteo-climatic conditions occurring at the study site.

1 Introduction

Monitoring the levels of radionuclides within the Arctic environment is important to help understanding the pathways for radionuclide transport to, within and from the Arctic (Chun, 2014; AMAP, 2010). Natural Occurring Radioactive Materials (NORMs) are nuclides strictly related to geologic sources and cosmogenic processes, which can describe air-masses origin and residence time (Baskaran, 2016). This is a key information for studying the fate of pollutants in the Arctic region, which is controlled by the meteo-climatic conditions occurring in the different seasons and in the different days of the year (Baskaran and Shaw, 2001). From a seasonal point of view, the extension of the so-called *"Arctic front"* (Stohl, 2006) can deflect, in fact, air masses originated in continental areas (such as Northern Europe, Russia, Asia and North America) to higher altitudes, reducing the contribute to the deposition processes. Radon and its progeny represent an important tracer of the meteo-climatic conditions occurring in the lower atmosphere. The use of NORMs, and in particular of radon, for pollution purposes was extensively investigated at lower latitudes (Duenas et al., 1996; Perrino et al., 2001; Sesana et al., 2003; Chambers et al., 2011; 2015), especially in urban settings. These case studies support the scientific community to use ^{222}Rn as a comparatively simple and economical approach for defining the stability conditions of the lower troposphere and for estimating the mixing height

(Pasini and Ameli, 2003; Sesana et al., 2003; Veleva et al., 2010; Griffith et al., 2013; Pasini et al., 2014; Salzano et al., 2016). The low emissive conditions of the ground, controlled by the permafrost dynamics, limit the application of this approach in polar regions. The requirement of significant low levels of detection (LLD) can, in fact, be bypassed only having high-volume sampling and/or high-sensitivity detectors (Chambers et al 2014). The available techniques can be classified considering the half-life ($t_{1/2}$) of the considered isotopes: the direct measurement of radon nuclides (^{222}Rn or ^{220}Rn) detecting the in-equilibrium progeny (^{218}Po and ^{216}Po with $t_{1/2} < 5\ min$); the indirect techniques based on the detection of short-lived isotopes (such as ^{214}Bi and ^{214}Pb with $t_{1/2} < 1\ hour$) and of long-lived nuclides (such as ^{212}Bi, ^{212}Pb with $1 < t_{1/2} < 10\ hours$); and the indirect methods based on the detection of near-constant progeny (such as ^{210}Pb and ^{210}Bi with $t_{1/2} > 1\ day$). All of these techniques are based on the chemical behavior of radon: it is a noble gas that, once emitted by soil, leaves the surface by molecular diffusion or by convection, and enters the atmosphere where it is distributed by turbulent mixing (Porstendorfer, 1994). This gas is chemically unreactive and a negligible amount can be adsorbed on particles by physi-sorption through electrostatic attraction (Bocanegra and Hopke, 1988). On the other hand, the radon decay products (^{222}Rn and ^{220}Rn have $t_{1/2}$, respectively, of about 3.8 days and 55 s) are metallic elements that are easily fixed to existing aerosol particles in the atmosphere. The reduction of these particles in the atmosphere occurs either by radioactive decay or by removal processes (dry deposition, rainout, washout). The distribution of this aerosol component in the troposphere is controlled mainly by turbulent mixing.

Different techniques were developed for the estimation of this important tracer considering the physical behavior and/or the decay chain of this gas. The most common "*direct*" measurement of Rn is based on the collection of ^{218}Po by electrodeposition coupled to alpha-particle detection (Wada et al., 2010). Furthermore, the lowest detection limit (up to 70 mBq m^{-3}) can be obtained isolating the gaseous phase, removing the ^{220}Rn component and detecting the freshly-decayed metals (Chambers et al., 2011). Looking at the "*indirect*" measurement of Rn on particulate matter, the most common approach is based on collecting and counting the total activity associated with S_β and L_β (Perrino et al., 2000; Salzano et al., 2016). This picture is completed, in conclusion, by the determination of C_β, where the collection and the detection steps can be separated and samples can be stored for a significant time (Paatero et al., 2010). Considering advantages or disadvantages, the lowest detection limits can be obtained having a complex sampling/counting system that is difficult to deploy and maintain in remote conditions. The "*indirect*" methods have a reduced impact in terms of resources necessaries for the installation and for maintenance but they require the assumption of equilibrium between radon gas and its aerosol progeny. This assumption is generally considered to be valid for sites that are at a significant distance from the radon terrestrial source, if weather conditions are fairly calm, but is likely to fail during precipitation episodes and under severe-sea conditions. This study will focus the attention on the technique based on the not-in-equilibrium progeny (S_β, L_β and C_β), where high-volume sampling is not required. This is a single-filter approach coupled to beta-counting and it represents, at the moment, the best compromise between detection efficiency and required resources. Furthermore, the disequilibrium issue is less invasive compared with the most common approach available in literature about the Arctic region (Zhang et al., 2015), where near-constant progeny is involved.

Atmos. Chem. Phys. Discuss., https://doi.org/10.5194/acp-2017-668
Manuscript under review for journal Atmos. Chem. Phys.
Discussion started: 1 August 2017

Atmospheric Chemistry and Physics Discussions

The present study tests the potentiality to study hourly variations instead of daily samples. Seasonal trends have been already investigated and the role of the Arctic haze on radon and its progeny has been already highlighted (Suzuki et al., 1996; Paatero et al., 2010; Zhang et al., 2015). We will describe the high-frequency behavior of radon progeny looking at the persistence of stability conditions and we will combine these results with the air-mass characterization based on back-trajectories.

2 Methods

The study was carried out at the Gruvebadet observatory, facility of the Arctic Station "Dirigibile Italia" located in Ny Ålesund, Spitzbergen (79°N, 11°E, 50 m a.s.l.). The site (Fig. 1) is located in the Brøgger Peninsula that is NW-SE oriented in front of the Kongsfjorden. Different glacial valleys (Austre - Midtre - Vestre Lovénbreen, Austre Brøggerbreen, etc.) slope down from the reliefs where the highest altitude is 1017 m above the sea level. Additional facilities are available nearby for the characterization of the physical conditions of the lower atmospheric boundary layer. The survey covered the period from 1 April to 28 October 2015, including the melting season and the entire summer season.

2.1 Radon progeny

The natural radioactivity was measured using an automatic stability monitor (PBL Mixing Monitor, FAI Instruments, Fontenuova, Rome, Italy) with a sampling height of 3 m above the ground. The system comprises an air sampler for the collection of particulate matter on filter membranes and a Geiger-Muller counter for determining the total β activity of radionuclides attached to the particles. The instrument operates on two filters at the same time: while the sampling phase is acting on one filter for 1 h, the β detection is performed on the other filter at four different intervals (0-10, 10-20, 30-40, 40-50 minutes). These instrumental features ensure that the β activity of the particles is continuously determined over an integration time of 1 h and that the β measurement period is long enough to guarantee highly accurate results. The accuracy of the determination is improved by the automatic subtraction of the background radiation (Perrino et al., 2000) and the maximum instrumental error at the lowest counting level was about 8%. T_β in Eq. (1) is the sum of β particles emitted by different nuclides sampled in the aerosol ($[N]_\beta^i$):

$$T_\beta = \sum_{i=1}^{n} [N]_\beta^i \quad (1)$$

Each nuclide is collected on the filter after a sampling period and is detected during a counting interval. Both phases are regulated by differential equations (Islam and Haque, 1994) and the sampling phase can be generalized as:

$$\frac{d[N]_s^i}{dt} = \nu[N]_{air}^i + \lambda_{i-1}[N]_s^{i-1} - \lambda_i[N]_s^i \quad (2)$$

where the first term on the right side represents the collection obtained specifying the air sampling flow rate (ν) in $m^3\ h^{-1}$ and activity in the air ($[N]_{air}^i$). The second term defines the contribution of the eventually-occurring parent isotope (i-1) on the filter and the third term is the decay component of the daughter nuclide (i). Those decay terms considers the specific decay

Atmos. Chem. Phys. Discuss., https://doi.org/10.5194/acp-2017-668
Manuscript under review for journal Atmos. Chem. Phys.
Discussion started: 1 August 2017

constant of the parent (λ_{i-1}) and daughter (λ_i) isotopes. Furthermore, the presence of the nuclide in the air is described in Eq. (3) by the combination of the locally originated nuclide ($[N]_L^i$) added to transported contribute ($[N]_T^i$).

$$[N]_{air}^i = [N]_L^i + [N]_T^i \quad (3)$$

The counting phases are described by similar differential equations where emitting is controlled by the daughter decay and the eventual supply of the parent nuclide:

$$\frac{d[N]_\beta^i}{dt} = \lambda_{i-1}[N]_s^{i-1} - \lambda_i[N]_s^i \quad (4)$$

Considering only NORMs, Eq. (1) can be described by the sum of β emissions produced by ^{222}Rn progeny (S_β), ^{220}Rn progeny (L_β) and some near-constant nuclides including cosmogenic isotopes (C_β).

$$T_\beta = S_\beta + L_\beta + C_\beta \quad (5)$$

Excluding from C_β the contribution of ^{210}Pb, due to the low β energy emission ($E_\beta < 100\ keV$) where the detector has a very low efficiency (Lee and Burgess, 2014), the remaining near-constant nuclides are ^{210}Bi ($t_{1/2} \sim 5\ days$ and $E_\beta \sim 1162\ keV$), ^{10}Be ($t_{1/2} > 10^6\ years$ and $E_\beta \sim 556\ keV$) and ^{14}C ($t_{1/2} \sim 5700\ years$ and $E_\beta \sim 156\ keV$). While the ^{14}C contribution is limited by the low efficiency of detectors at low energies and by the limited amount of carbon present on filters (below 1 μg m^{-3}), the ^{10}Be component is limited by the low activities present in the atmosphere. Summarizing, we have one rapid-decay component (S_β decreases 60 - 70 % within one hour) and one near-constant member (C_β). The intermediate term (L_β) reduces its activity to about 5 - 15 % after one hour. The mixing between those three components defines the final decay behavior observable at an hourly scale with four different counting steps. We can have two different seasonal behaviors in the Arctic region: one occurring especially during the Arctic winter, when the local emission of radon (both ^{222}Rn and ^{220}Rn) is negligible ($L_\beta \simeq 0$) and the residence time of aerosol over sea (more than 2 days) is higher in presence of the so-called "Arctic haze" ($C_\beta \simeq [^{210}Bi]_\beta$); one occurring especially in the summer, when the local component is significant and the Arctic haze is reduced ($S_\beta \gg L_\beta > C_\beta$). We assume under both conditions that transient equilibrium is occurring between the two progenies ($[^{214}Pb]_{air} = [^{214}Bi]_{air}$ and $[^{212}Pb]_{air} = [^{212}Bi]_{air}$). Some bias can occur especially during the summer when the local source is dominating over transport and the disequilibrium between progenies can be significant.

The above mentioned differential equation Eq. (2), concerning the sampling phase, can be solved using the Bateman's solutions, considering the two seasonal assumptions:

$$[^{214}Bi]_\beta = 1.51[^{214}Pb]_\beta \quad (6a)$$

$$[^{214}Pb]_{air} = 1.97\ \nu^{-1}\ [^{214}Pb]_\beta \quad (6b)$$

$$[^{212}Bi]_\beta = 1.02[^{212}Pb]_\beta \quad (6c)$$

$$[^{212}Pb]_{air} = 1.03\ \nu^{-1}\ [^{212}Pb]_\beta \quad (6d)$$

$$[^{210}Bi]_{air} = \nu^{-1}\ [^{210}Bi]_\beta \quad (6e)$$

Atmos. Chem. Phys. Discuss., https://doi.org/10.5194/acp-2017-668
Manuscript under review for journal Atmos. Chem. Phys.
Discussion started: 1 August 2017

Atmospheric Chemistry and Physics Discussions

The Eq. (4) regarding the counting intervals must be solved for each period. The solution must consider the first and the last counting periods: from 0 to 10 minutes (first interval T_β^1) and from 40 to 50 minutes (forth interval T_β^4) after the end of the air sampling.

$$T_\beta^1 = \epsilon_{1024}[^{214}Pb]_\beta d_1^1 + \epsilon_{3272}[^{214}Bi]_\beta d_2^1 + \epsilon_{570}[^{212}Pb]_\beta d_3^1 + \epsilon_{2252}[^{212}Bi]_\beta d_4^1 + C_\beta \quad (7a)$$

$$T_\beta^4 = \epsilon_{1024}[^{214}Pb]_\beta d_1^4 + \epsilon_{3272}[^{214}Bi]_\beta d_2^4 + \epsilon_{570}[^{212}Pb]_\beta d_3^4 + \epsilon_{2252}[^{212}Bi]_\beta d_4^4 + C_\beta \quad (7b)$$

The coefficients in Eq. (7a and 7b) are the detector efficiencies at each energy (ϵ_{keV}) and the decay parameters (d_i^n) obtained solving exponential equations for each ith isotope at each nth counting interval. We were not able to determine routinely the detector efficiency at each energy but it was possible to make some experiments with a similar instrument and some reference materials such as a KCl standard (we prepared a known ^{40}K filter with $E_\beta \sim 1311\ keV$) and a ^{137}Cs-contaminated soil (we prepared a ^{137}Cs-enriched filter with $E_\beta \sim 531\ keV$ where the activity was determined by γ-spectrometry). This preliminary calibration requires a stronger effort for estimating precisely the efficiency at different energies but a relative ratio between the detector efficiency at 570, 1024 and 2252 keV normalized to the efficiency at 1024 keV was estimated in order to study the variations of the three β-emitting components (S_β, L_β and C_β). We found that $\epsilon_{570} \sim 0.41\epsilon_{1024}$, $\epsilon_{1162} \sim 1.1\epsilon_{1024}$, $\epsilon_{2252} \sim 1.8\epsilon_{1024}$ and $\epsilon_{3272} \sim 2.1\epsilon_{1024}$. Substituting these parameters to Eq. (7a and 7b) and solving the system including a ^{220}Rn to ^{222}Rn ratio (f), we obtained:

$$S_\beta = 1.97 \frac{(N_{\beta,1} - N_{\beta,4})}{(2.15 + 0.74f)} \nu^{-1} \quad (9a)$$

$$L_\beta = 3.74f \frac{(N_{\beta,1} - N_{\beta,4})}{(2.15 + 0.74f)} \nu^{-1} \quad (9b)$$

$$C_\beta = [N_{\beta,4} \frac{(2.14f + 1.89)}{(2.15 + 0.74f)} (N_{\beta,1} - N_{\beta,4})] \nu^{-1} \quad (9c)$$

where both quantities are expressed in cps m^{-3}. The estimation of the three components was obtained minimizing the chi-squared indicator, calculated between the four counting intervals and the respective values simulated between the two end-member situations ($C_\beta = 0$ and $L_\beta = 0$). The optimization algorithm was developed in the R-Project programming environment (R Core Team, 2016). The lower limit of detection, in terms of ^{222}Rn, of the stability monitor was estimated at 0.15 Bq m^{-3} (Salzano et al, 2016). Considering the logistic restrictions of the study site, routine quality check and sampling efficiency assessments were not possible. These limitations forced us to express the three components in terms of relative radioactivity (cps m^{-3}) with a LLD of 0.0035, 0.013 and 0.0072 cps m^{-3}, respectively.

2.2 Soil Rn-flux

The estimation of the soil Rn flux (ϕ) was obtained using a stationary model where the major controlling factors are the soil radon emanation power and the soil water saturation (Zhuo et al., 2008). The model, based on Equation 10, required as input parameters the soil temperature (T_S), the soil water content (S), the soil Ra content (R), the soil density (ρ_b) and the soil porosity

(p). In addition to some constants that are included, such as the radon decay constant (λ) and the diffusion coefficient of radon in the air (D_0), the emanation power (ε) can be calculated following the equations described by Zhuo et al. (2008).

$$\phi = R\rho_b\varepsilon\left(\frac{Ts}{273}\right)^{0.75}\sqrt{\lambda D_0 p e^{-6Sp-6S^{14p}}} \quad (10)$$

Compared to the preliminary description presented in Salzano et al. (2016), the description of the soil thaw depth is a critical input parameter in cold regions. Permafrost can be idealized as a two-layer system where the upper active layer overlays a frozen water-saturated layer. From this perspective, we approached the problem considering the 9 m temperature profile provided by the Bayelva borehole (Paulik et al., 2014), which supported also the estimation of the average temperature of the active layer. The developed model is a simplified solution that could be influenced by under-prediction under unsteady conditions. Appropriate validating activities are required in order to evaluate the performance of this model. The estimation of the soil water content was approached using remotely sensed data provided by the EUMETSAT organization. We selected the soil moisture product obtained by the ASCAT sensor, which is a real-aperture radar operating at 5.255 GHz (C-band) (EUMETSAT, 2015).

2.3 Back trajectories

The analysis of the back trajectories was approached calculating the air mass path with the HYSPLIT model (Stein et al., 2015). We considered 5 days' trajectories using the GDAS meteorological dataset. Simulations were targeted on the study site at different altitudes (500 and 1000 m a.s.l.) in order to evaluate the influence of orography on trajectories.

3 Results

Two different questions were approached in order to evaluate the potentialities in using radon-progeny in the Arctic region: what is the impact of permafrost dynamics on the radon detection in the air? How does the air mass trajectory control the signal detected in the lower atmosphere?

3.1 The contribution of the local soil flux to the air concentration

The evolution of the three radioactive components (Fig. 2a) seemed to be produced by the overlapping of different sources and processes. All of these factors can have different seasonal behaviors and this issue highlighted the need of a time-series analysis. The first step consisted, in fact, in de-trending the time series isolating the local-source component, which is controlled by the emissive condition of the local surface. The remaining seasonal components (distinct in low and high emanation periods) where analyzed removing the high-frequency bias (daily oscillations) using a smoothing procedure based on a centered weighted moving average with a 24-hours window (Cowpertwait and Metcalfe, 2009). The main feature distinguishing the identified periods was the amplitude of variations concerning the natural radioactivity. While small fluctuations (up to 0.1 cps m^{-3}) in S_β were detected during the low-emanation period, L_β seemed to be quite negligible and C_β was frequently detected. The high-emanation period was characterized by sharp variations up to 0.8 cps m^{-3} in terms of S_β, by

significant variations concerning L_β and by an occasionally detectable amount of C_β. The presence of L_β and C_β showed also a specific behavior: while L_β followed the trend described by S_β (0.018 ± 0.013 cps m^{-3} in the first period and 0.06 ± 0.01 cps m^{-3} in the second one), C_β showed the opposite (0.009 ± 0.007 cps m^{-3} in the first period and 0.007 ± 0.007 cps m^{-3} in the second one).

Furthermore, looking at peaks defined by values higher than the third quartile, different episodes can be identified for each progeny component during each emanation period. While the S_β and the L_β components showed episodes that are significantly matching in terms of maxima, especially during the high-emanation period (r^2 = 0.79), C_β showed peaks completely independent from the other components. The interpretation of the observed seasonality in the time-series is supported by the reconstruction of an indicative soil Rn-flux (Fig. 2b). The two different emanation periods can be identified also looking at the soil Rn exhalation rate, which is controlled by the thermal behavior of the permafrost layer. The presented model output required two important input parameters (the thickness of the active layer and the average soil temperature) obtained from borehole measurements at the surface and from the remotely-observed water saturation of the ground. The final output of the stationary emanation model indicated a limited soil emission until the end of May with a maximal emissive condition of local soils reached after 30 days at the beginning of July. Referring to the impact of permafrost dynamics, we can distinguish between a low-emanation period (which includes the ablation, the fusion and active-layer development phases) and a high-emanation period (as soon as the ground reached the maximal thickness of the emanating active-layer). The transition between the two periods can be positioned approximately in 8-9 July 2015 within a very short time interval. The observed abrupt impact of soil emanation on natural radioactivity in the air is coherent with the expected stabilization of soil exhalation obtained from the model. This consistency implies that atmospheric processes are influenced by a regional source where emissive conditions of the ground are mostly stabilized. The model output is, in fact, representative only for the Ny Ålesund site as permafrost observations are site-specific (the study area is a coastal zone) and they cannot describe the overall behavior of more internal areas where orography is very complex.

3.2 The contribution of the meteo-climatic conditions to the air concentration

The combination between the three components could represent a diagnostic tool capable to describe the meteo-climatic conditions occurred on air masses. Looking at the occurrence of isotopic mixtures with different relative percentage of each component (Fig. 3a), the most frequent situation during both emanation periods (Fig. 3b) was, of course, the condition dominated by the short-lived progeny (HiS), with a frequency ranged between 72% and 78%. The most significant difference between the two periods was represented by the partition of contributions between the near-constant (CS and SC) and the long-lived (HiL and SL) classes. While the intermediate conditions between S_β and C_β were more consistent during the low emanation period (respectively about 7% and 2%), the terms between S_β and L_β were almost dominant during the second period (respectively about 15% and 26%). The first behavior is consistent with the end of the Arctic winter, when the arctic haze enriches polar air masses with nuclides such as ^{210}Pb and consequently ^{210}Bi (Zhang et al., 2015). Furthermore, those conditions could highlight the occurrence of "*old*" air masses that were persistent at higher latitudes where radon sources are negligible.

On the other hand, the presence of L_β could trace the contribution of local sources or the arrival of recently emitted air masses (this component has a limited residence time in the atmosphere due to its complete decay reached after 50 hours). The importance of detecting these different components consists in the possibility to estimate the "*age*" and the "*origin*" of air masses (Chun, 2014). The relationship between each radon-progeny mixture and the wind features highlighted (Fig. 3c) that HiL situations were strictly controlled by the occurrence of calm condition. Furthermore, this was particularly evident during the summer period with an occurrence of about 60%. On the other hand, this relation, observed also on the C_β-dominated mixtures, supports that low wind-speed conditions favor the accumulation of nuclides (atmospheric stability) compared to advective situations that moved all the components to the specific lower limits of detection. The study site is influenced deeply by orographic effects and can be described as a system that might be heavily stratified (Di Liberto et al., 2012; Mazzola et al., 2016). The role of wind-calm conditions was relevant if we consider that accumulation of nuclides is favored by near-stable conditions of the lower atmosphere. From this perspective, we can infer that S_β and L_β are coexistent when local emission and atmospheric stability are dominant compared to long-range transport. This last process can be identified when L_β is negligible (^{212}Pb and ^{212}Bi is completely decayed after 50 hours) and air masses could be "*recent*" or "*aged*" in presence or not, respectively, of S_β.

This interpretation can be supported describing two case-study situations (Fig. 4). The first example shows the contribute of processes related to long-range transport. We observed two advective phases (when wind speed was higher than 1 m s^{-1} before 1 May) followed by a relatively-stable situation. The L_β increased (about 20%), especially during the third phase, evidencing that, although the emanation conditions of the ground were unfavorable during all the period, the radon emanation was not negligible. All of the air masses were persistent over the Arctic Ocean for at least 5 days and the contact with terrestrial surfaces is significant only in the third phase. While the overpass on Svalbard was limited to 10-20 hours in the first two situations, the third phase, dominated by atmospheric stability (wind-calm), was characterized by a persistence over the islands of about 48 hours including a heavy compression episode occurring close to coast 24 hours before the contact in Ny Ålesund. The difference between the first two phases could be represented by the stratification of the atmosphere close to the study site. While the first phase was characterized by a homogeneous flying altitude of the air mass, the second situation was influenced by the rise of sea-lying air masses potentially depleted of haze-related isotopes. While mixtures of the first phase lay in between SC and CS classes, the second and the third ones can be classified as HiL with a decreasing short-to-long progenies ratio. This feature controlled the presence of L_β close to the measuring station and the absence of C_β at lower altitudes above the continental areas. The occurrence of near-stable conditions in the atmosphere controls, moreover, the accumulation of nuclides. This behavior was slightly visible when emanation is very low, but it was clearly identified in the second episode occurring between June 6 and 11 (Fig. 4). The accumulation of S_β and L_β was, in this case, consistent with near-stable conditions of the lower atmosphere and potential emitting areas are 50 hours far from the measuring station. The peak situation can be classified as SL indicating that the short-to-long ratio is proportional to the contribute of long-range transport, of "*recent*" air masses (originated up to 20 days before), instead of local emission. This statement is supported by this example thus the considered

air mass was over continental areas at lower latitudes and altitudes 3-4 days before the contact with Ny Ålesund. The presence of C_{β} cannot be investigated at this stage of the study due to the very long residence time of those nuclides in the atmosphere. The availability of a longer dataset is the first step that must be addressed in order to approach this issue.

4 Conclusions

The detection of β emission from airborne particles with a high-time resolution offers the opportunity to increase the capability of studying atmospheric processes in polar areas. The reduction of soil exhalation during spring may appear as a limitation, but it represents an important challenge. The composition of the radon progeny, defined for the first time with a high-time resolution, supported the identification of air masses dominated by long-range transport (with life up to 20 days and more than 20 days) in presence or not of near-constant radionuclides instead of long and short lived progenies. This study supports to extend this approach from the definition of the accumulation processes involving isotopes present in the lower atmosphere, to the identification of the stability conditions of the lower atmosphere, to gather information about air masses and the soil-exhalation conditions. Two different emanation periods were defined in accordance to the permafrost occurrence at the ground. Furthermore, accumulation windows were recognized coherently to the meteo-climatic conditions occurring at the study site. This preliminary attempt must be continued with a longer time series in order to statistically analyze the correlation between radioactivity and mixing state of the lower atmosphere. However, we are confident that coupling this method with traditional chemical determinations on gases and aerosols, a more complete picture of pollutant dynamics in the Arctic region can be achieved.

5 Acknowledgments and Data

This study was supported by the logistic service provided by the Earth System Science and Environmental Technologies Department of the National Research Council of Italy. We would like to thank EUMETSAT for providing data products concerning the soil moisture content and AWI for the available dataset about the permafrost thermal profile. The authors gratefully acknowledge the NOAA Air Resources Laboratory (ARL), for the provision of the HYSPLIT transport and dispersion model used in this publication, and NCEP, for providing the Global Data Assimilation System (GDAS). This manuscript was language-proofed by Lena Rettori.

References

AMAP: AMAP Assessment 2009: Radioactivity in the Arctic. Arctic Monitoring and Assessment Programme (AMAP), Oslo, Norway, ISBN 13 978-82-7971-059-2, 2010.

Baskaran M.: Radon: A Tracer for Atmospheric Studies, in Radon: A Tracer for Geological, Geophysical and Geochemical Studies, Springer, Switzerland, 63-81, doi:10.1007/978-3-319-21329-3, 2016.

Baskaran M., and Shaw G. E.: Residence time of arctic haze aerosols using the concentrations and activity ratios of Po, Pb and Be, Aerosol Sci., 32, 443-452, 2001.

Bocanegra R., and Hopke P. K.: Radon adsorption on activated carbon and the effect of some airborne contaminants, Sci. Total Environ., 76, 193-202, doi:0048-9697/88/$03.50, 1988.

Chambers S. D., Hong S. B., Williams A. G., Crawford J., Griffiths A. D., and Park S. J.: Characterising terrestrial influences on Antarctic air masses using Radon-222 measurements at King George Island, Atmos. Chem. Phys., 14, 9903–9916, 2014.

Chambers S. D., Williams A. G., Crawford J., and Griffiths A. D.: On the use of radon for quantifying the effects of atmospheric stability on urban emissions, Atmos. Chem. Phys., 15, 1175–1190, 2015.

Chambers S. D., Williams A. G., Zahorowski W., Griffiths A. D., and Crawford J.: Separating remote fetch and local mixing influences on vertical radon measurements in the lower atmosphere, Tellus, Ser. B, 63, 843–859, 2011.

Chun J.: On the research needed to better characterise natural radioactivity accumulated in the Arctic by long-range atmospheric transport, Radiat. Prot. Dosim., 158(4), 369 –372, 2014.

Cowpertwait P. S. P., and Metacalfe A. V.: Introductory Time Series with R (2nd Ed), Springer, Baltimore, USA, doi:10.1007/978-0-387-88698-5, 2009.

Di Liberto L., Angelini F., Pietroni I., Cairo F., Di Donfrancesco G., Viola A., Argentini S., Fierli F., Gobbi G., Maturilli M., Neuber R., and Snels M.: Estimate of the Arctic Convective Boundary Layer Height from Lidar Observations: A Case Study, Adv. Meteorol., 2012, 851927, doi:10.1155/2012/851927, 2012.

Duenas C., Perez M., Fernandez M. C., and Carretero J.: Radon concentrations in surface air and vertical atmospheric stability of the lower atmosphere, J. Environ. Radioact., 31, 87–102, 1996.

EUMETSAT: ASCAT Product Guide, EUM/OPS-EPS/MAN/04/0028, 2015.

Griffith A. D., Parkes S. D., Chambers S. D., McCabe M. F., and Williams A. G.: Improved mixing height monitoring through a combination of lidar and radon measurements, Atmos. Meas. Tech., 6, 207–218, 2013.

Islam G. S., and Haque A. K. F.: Measurement of mixed radon and thoron daughter concentrations using alpha and beta activities filtered from air, Radiat. Meas., 23(4), 737–742, 1994.

Lee C. J., and Burgess P. H.: The examination, testing and calibration of portable radiation protection instruments, Measurement Good Practice Guide, 14, NPL, Teddington, UK, 2014.

Mazzola M., Tampieri F., Viola A. P., Lanconelli C., and Choi T.: Stable boundary layer vertical scales in the Arctic: observations and analyses at Ny-Alesund, Svalbard, Q. J. R. Meteorol. Soc., 142, 1250–1258, doi:10.1002/qj.2727, 2016.

Paatero J., Buyukay M., Holmén K., Hatakka J., and Viisanen Y.: Seasonal variation and source areas of airborne lead-210 at Ny-Ålesund in the High Arctic, Polar Res., 29, 345–352, 2010.

Pasini A., and Ameli F.: Radon short range forecasting through time series preprocessing and neural network modeling, Geophys. Res. Lett., 30(7), 1386, 2003.

Pasini A., Salzano R., and Attanasio A.: Modeling radon behavior for characterizing and forecasting geophysical variables at the atmosphere-soil interface, in Recent trends in modelling of environmental contaminants, edited by D. Sengupta, Springer, New Delhi, 213–237, 2014.

Paulik C., Melzer T., Hahn S., Bartsch A., Heim B., Elger K., and Wagner W.: Circumpolar surface soil moisture and freeze/thaw surface status remote sensing products (version 4) with links to geotiff images and NetCDF files (2007-01 to 2013-12). Department of Geodesy and Geoinformatics, TU Vienna, doi:10.1594/PANGAEA.832153, 2014.

Perrino C., Febo A., and Allegrini I.: A new beta gauge monitor for the measurement of PM10 air concentration, in EMEP-WMO workshop on fine particles—emissions, modelling and measurements, edited by J. E. Hanssen, EMEP/CCC-Report 9/2000, NILU, Kjeller, 147–152, 2000.

Perrino C., Pietrodangelo A., and Febo A.: An atmospheric stability index based on radon progeny measurements for the evaluation of primary urban pollution, Atmos. Environ., 35(31), 5235–5244, 2001.

Porstendorfer J.: Properties and behaviour of radon and thoron and their decay products in the air, J. Aerosol Sci., 25(2), 219–263, 1994.

Salzano R., Pasini A., Casasanta G., Cacciani M., and Perrino C.: Quantitative Interpretation of Air Radon Progeny Fluctuations in Terms of Stability Conditions in the Atmospheric Boundary Layer, Bound-Lay. Meteorol., 160(3), 529–550, doi:10.1007/s10546-016-0149-6, 2016.

Sesana L., Caprioli E., and Marcazzan G. M.: Long period study of outdoor radon concentration in Milan and correlation between its temporal variations and dispersion properties of atmosphere, J. Environ. Radioact., 65, 147–160, 2003.

Stein A. F., Draxler R. R., Rolph G. D., Stunder B. J. B., Cohen M. D., and Ngan F.: NOAA's HYSPLIT atmospheric transport and dispersion modeling system, Bull. Amer. Meteor. Soc., 96, 2059-2077, doi:10.1175/BAMS-D-14-00110.1, 2015.

Sthol A.: Characteristics of atmospheric transport into the Arctic troposphere, J. Geophys. Res., 111, D11306, doi:10.1029/2005JD006888, 2006.

Suzuki T., Nakayama N., Igarashi M., Kamiyama K., and Watanabe O.: Concentrations of 210Pb and 218Po in the atmosphere of Ny-Alesund, Svalbard, Mem. Natl Inst. Polar Res., Spec. Issue, 51, 233-237, 1996.

Veleva B., Valkov N., Batchvarova E., and Kolarova M.: Variation of short-lived beta radionuclide (radon progeny) concentrations and the mixing processes in the atmospheric boundary layer, J. Environ. Radioact., 101, 538–543, 2010.

Zhang W., Chen J., Ungar K., and Cooke M.: Estimation of the Arctic aerosols from local and long-range transport using relationships between 210Pb and 212Pb atmospheric activity concentrations, J. Environ. Radioact., 141, 123-129, doi:10.1016/j.jenvrad.2014.12.008, 2015.

Zhuo W., Guo Q., Chen B., and Cheng G.: Estimating the amount and distribution of radon flux density from the soil surface in China, J. Environ. Radioact., 99, 1143–1148, 2008.

Atmos. Chem. Phys. Discuss., https://doi.org/10.5194/acp-2017-668
Manuscript under review for journal Atmos. Chem. Phys.
Discussion started: 1 August 2017

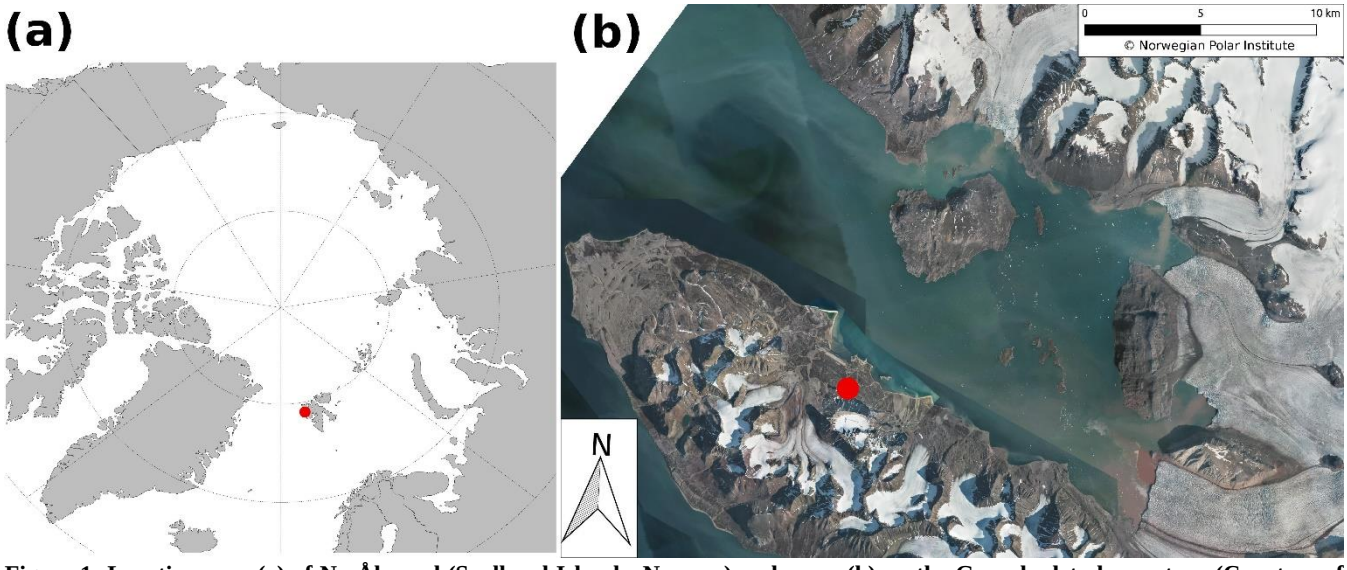

Figure 1: Location map (a) of Ny Ålesund (Svalbard Islands, Norway) and zoom (b) on the Gruvebadet observatory (Courtesy of Norwegian Polar Institute).

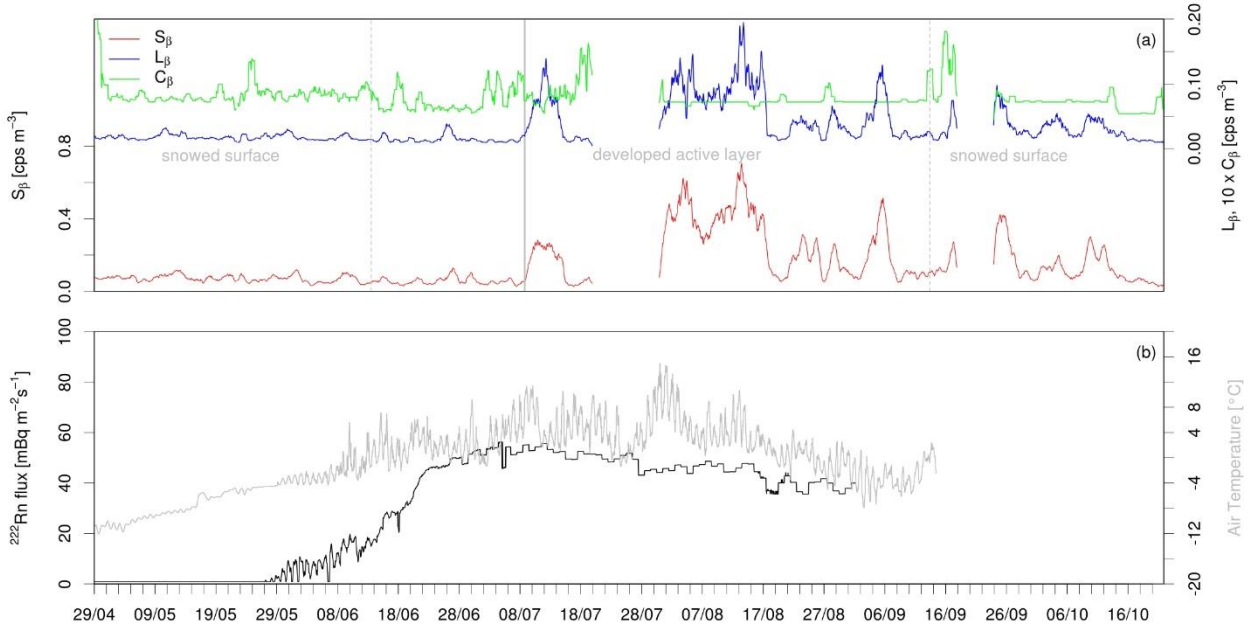

Figure 2: Soil flux (black line) versus airborne natural radioactivity (colored lines) in Ny Ålesund. The air temperature (grey) was measured at the CCT Tower facility.

Atmos. Chem. Phys. Discuss., https://doi.org/10.5194/acp-2017-668
Manuscript under review for journal Atmos. Chem. Phys.
Discussion started: 1 August 2017

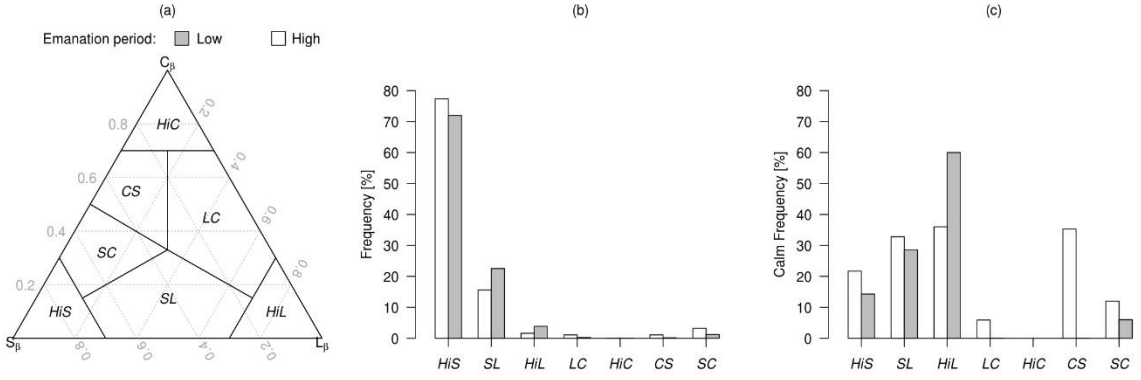

Figure 3: Classification of radon-progeny mixtures (a), occurrence of the different isotopic compositions (b) and association between the different mixtures under wind-calm conditions (c). Classes were defined considering the relative amount of each component.

Atmos. Chem. Phys. Discuss., https://doi.org/10.5194/acp-2017-668
Manuscript under review for journal Atmos. Chem. Phys.
Discussion started: 1 August 2017

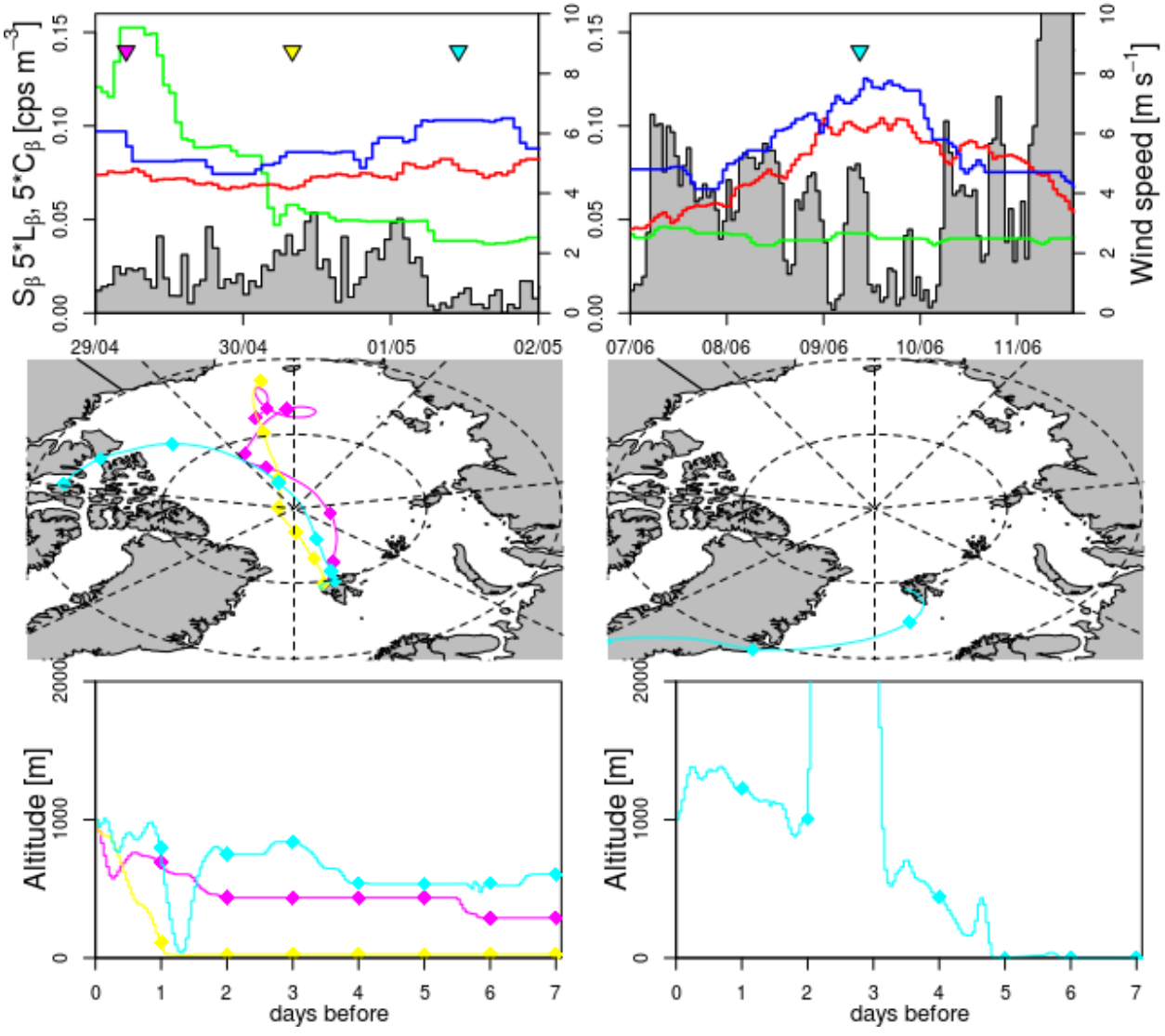

Figure 4: Evolution of the isotopic composition of radon progeny compared to wind conditions (top), specific back-trajectories in terms of path (middle) and altitude (bottom). One example is referred to long-range transport at the beginning of the melting season (left) and one to local emission (right).